TÜBİTAK

Turkish Journal of Chemistry

http://journals.tubitak.gov.tr/chem/

Research Article

Turk J Chem
(2016) 40: 76 – 92
© TÜBİTAK
doi:10.3906/kim-1501-32

Synthesis and structural properties of N-3,4-(dichlorophenyl)-3-oxo-3-phenyl-2-(phenylcarbonyl)propanamide and its Cu(II) complex

Ahmet Oral SARIOĞLU[1], Tuğba TAŞKIN TOK[1,*], Mehmet AKKURT[2], Muhammad Nawaz TAHİR[3], Mehmet SÖNMEZ[1]

[1]Department of Chemistry, Faculty of Arts and Sciences, Gaziantep University, Şehitkamil, Gaziantep, Turkey

[2]Department of Physics, Faculty of Sciences, Erciyes University, Kayseri, Turkey

[3]Department of Physics, University of Sargodha, Sargodha, Pakistan

Received: 13.01.2015 • **Accepted/Published Online:** 12.07.2015 • **Final Version:** 05.01.2016

Abstract: A new N-carboxamide compound (**3**) was synthesized by the reaction of dibenzoylaceticacid-N-carboxyethylamide (**1**) and 3,4-dichloroaniline (**2**). The N-(3,4-dichlorophenyl)-3-oxo-3-phenyl-2-(phenylcarbonyl) propanamide (**3**) subsequently reacted with Cu salt to produce its Cu(II) complex compound (**4**). The compounds were characterized by analytical and spectral methods. In addition, X-ray diffraction was performed to characterize and obtain detailed information about the structure of **3**. The fully optimized geometries of compounds **3** and **4** were calculated at different basis sets by using the Gaussian09 (G09) software to investigate their 3D geometries and electronic structures. Comparisons between the calculated and experimental data including molecular structures, fundamental vibrational modes, and electronic properties were made. The comparisons showed that the theoretical data were compatible with the corresponding experimental values of compounds **3** and **4**.

Key words: Carboxamide, copper complex, X-ray, computational analysis

1. Introduction

Research on carboxamide compounds started with the identification of their chemical properties. Carboxamides play a key role in significant life processes such as protein formation.[1] When amides are conjugates with other aliphatic, aromatic, and heterocyclic rings various types of biological activity are produced. Recent reports have shown the importance of carboxamides in terms of anticonvulsant activity[2] in the search for new antagonists of excitatory amino acids receptors.

In the meantime, coordination chemistry of metal complexes derived from ligands involving carboxamide (–CONH–) nitrogen donors has received considerable current attention.[3–6] Moreover, transition metal complexes of carboxamides have a crucial role in a vast number of widely differing biological processes. The ligands have carboxamide chains and their metal chelates represent very important pharmacological activities.[7,8] There are several roles exhibited by carboxamide nitrogen in the chemistry of different coordination complexes. The binding of two carboxamido nitrogen atoms with copper centers was observed in prion protein.[9]

Several reports have mentioned that the computational method has become a worthy partner and complement to experimental studies. The computational ab initio method is widely used to simulate UV-Vis, IR, and

*Correspondence: ttaskin@gantep.edu.tr

NMR spectra. In the present study, *N*-(3,4-dichlorophenyl)-3-oxo-3-phenyl-2-(phenylcarbonyl)propanamide (**3**) was synthesized with dibenzoylaceticacid-*N*-carboxyethylamide (**1**)[10] and 3,4-dichloroaniline (**2**), for the reasons mentioned above. Compound **3** was characterized by elemental analysis, IR, UV-Vis, ^{1}H, APT NMR and LC-MS/MS spectroscopy. Furthermore, compound **3** was examined using X-ray diffraction to reinforce the proposed structure. The Cu(II) complex compound **4** was obtained by the reaction of the bidentate ligand **3** and $Cu(CH_3COO)_2.H_2O$. Moreover, compound **4** was characterized by elemental analysis, IR, UV-Vis spectral data, and magnetic measurements. Finally, the computational ab initio method was performed as a basis of comparison with the experimental and X-ray data for compounds **3** and **4**. Additionally, molecular electrostatic potential surface (MEPS) and the highest occupied molecular orbital (HOMO) and lowest unoccupied molecular orbital (LUMO) gap were calculated to investigate the electron density and predict the biochemical activity of the new *N*-carboxamide compound (**3**).

2. Results and discussion

2.1. Synthesis and characterization

Compound **3** was obtained through the reaction of dibenzoylaceticacid-*N*-carboxyethylamide (**1**) and 3,4-dichloroaniline (**2**) in toluene. Complex **4** was synthesized by reaction of *N*-(3,4-dichlorophenyl)-3-oxo-3-phenyl-2-(phenylcarbonyl) propanamide (**3**) with $Cu(CH_3COO)_2.H_2O$ in a chloroform and methanol mixture. The route for the synthesis of compounds **3** and **4** is shown in the Scheme. The characterization of **3** and **4** was carried out by elemental analysis, UV-Vis, IR, ^{1}H, APT NMR, and LS-MS/MS spectroscopy and magnetic measurements.

The ^{1}H and APT NMR spectra gave results compatible with the structure of *N*-(3,4-dichlorophenyl)-3-oxo-3-phenyl-2-(phenylcarbonyl) propanamide (**3**). In the ^{1}H NMR spectrum of **3** in DMSO-d_6, the aromatic protons appeared as a broad band at 6.74–8.20 ppm, –NH proton at 10.73 ppm, and –CH proton among three carbonyl groups at 3.40 ppm. Furthermore, the APT NMR spectrum easily showed us which types of carbon were in compound **3**. In particular, carbonyl carbon, which was neighbors with nitrogen, was observed at 192.75 ppm, and the other two carbonyl carbons appeared at 164.73 ppm in positive amplitude of the spectrum. The carbon atoms without hydrogen in benzene rings were observed at 125.74 and 131.64 ppm, and two C–Cl carbon atoms at 136.00 and 139.10 ppm. In negative amplitude of the APT NMR spectrum, there were two types of carbon atom including one hydrogen. One carbon atom including one hydrogen in benzene rings was located at 119.67, 120.78, 127.90, 128.86, 129.34, 129.56, 131.37, and 134.49 and the second one, C–H carbon, among three carbonyl carbons at 64.88 ppm. In summary, ^{1}H and APT NMR spectra of compound **3** provided the characteristic chemical shifts and confirmed the proposed structure. Due to the paramagnetic property of compound **4**, its ^{1}H and APT NMR spectra were not available. The IR spectral data of compound **3** showed the formation of the proposed structure by the appearance of new absorption bands at 3254 cm^{-1} (N–H), 3062 cm^{-1} (Ar), 1687, 1672, 1537 cm^{-1} (C=O), 1593–1448 cm^{-1} (C=C), and 816 cm^{-1} (Ph–Cl). Furthermore, the result of LC-MS/MS spectroscopy supported the proposed compound (**3**). After conversion of compound **3** to the complex compound **4**, the peaks of the N–H and C=O of amide vibrations disappeared. The IR spectrum of compound **4** clearly exhibited the formation of compound **4** by the appearance of new absorption bands at 3028 cm^{-1} (Ar), 1617 cm^{-1} (C=O), 1593–1448 cm^{-1} (C=C), 1513 cm^{-1} (C=N), and 811 cm^{-1} (Ph–Cl). Moreover, the complex compound **4** was paramagnetic, with a magnetic moment (μ_{eff}) value of 1.82 B.M. The magnetic moment value indicated that the complex had a square planar conformation with the Cu(II)

center.[11,12] Therefore, we can confirm that the complex compound **4** had a square planar geometry with the Cu(II) center, due to the IR spectrum and magnetic moment value.

Furthermore, UV-Vis spectra of compounds **3** and **4** in DMF are given in Figure 1. The data of **3** and **4** were very similar to each other because of their structural identity. However, the absorbance intensities of **3** and **4** were different. This indicates the formation of complex **4** from compound **3**. Their electronic spectra in DMF solutions along with bands assigned to $\pi \rightarrow \pi^*$ and n $\rightarrow \pi^*$ transitions also exhibited absorption maxima at 270 nm and 315 nm.

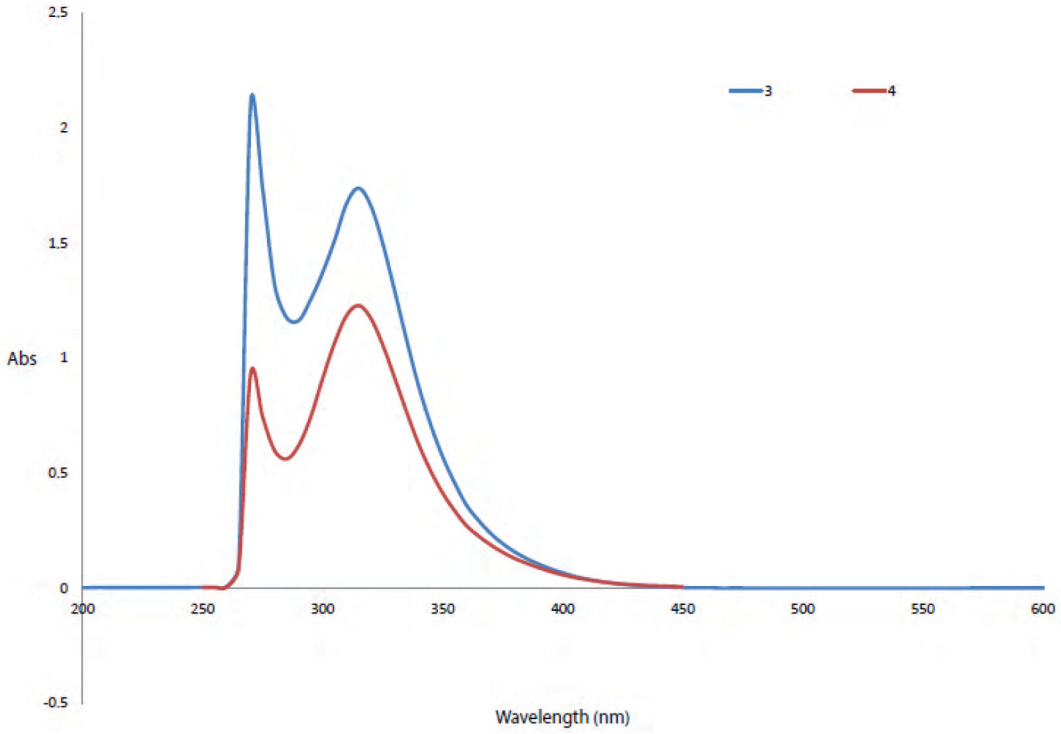

Figure 1. The UV-Vis spectra of compounds **3** and **4** in DMF.

2.2. X-ray crystallography results

As shown in Figure 2, the C17–C22 benzene ring of compound 3 with the two chlorine atoms attached makes dihedral angles of 71.62(14)° and 84.77(17)°, respectively, with the terminal phenyl rings (C1–C6 and C10–C15). These phenyl rings formed a dihedral angle of 77.85(18)° with each other.

All bond lengths and angles were within the normal range and were comparable to the corresponding values observed in similar structures.[13] The O1–C7–C8–C9, O1–C7–C8–C16, O2–C9–C8–C7, O2–C9–C8–C16, O3–C16–C8–C9, O3–C16–C8–C7, and O3–C16–N1–C17 torsion angles were –13.8(4)°, 105.2(3)°, –107.7(3)°, 11.3(4)°, –88.0(3)°, 33.1(4)°, and 3.7(5)°, respectively.

A weak intramolecular C–H...O interaction, which formed an S(6) ring, helped to establish the molecular conformation of compound 3 (Table 1).[14] In the crystal structure, neighboring molecules were linked by N–H...O and C–H...O hydrogen bonds, forming a three-dimensional network (Table 1; Figure 3). Furthermore, C–H... π interactions stabilized the crystal packing.

2.3. Computational results

As a first approach, we carried out the geometry optimization of compound **3** and complex compound **4**. The optimized compounds (**3** and **4**) were obtained representing the numbering scheme of the atoms with computational ab initio methods by using the G09 program (Figures 4 and 5). Parameters with bond lengths, bond angles, and dihedral angles of the optimized compounds (**3** and **4**) are listed in Tables S1–S7. The calculated data of compound **3** were also compatible with X-ray diffraction results as given in Tables S8–S10.

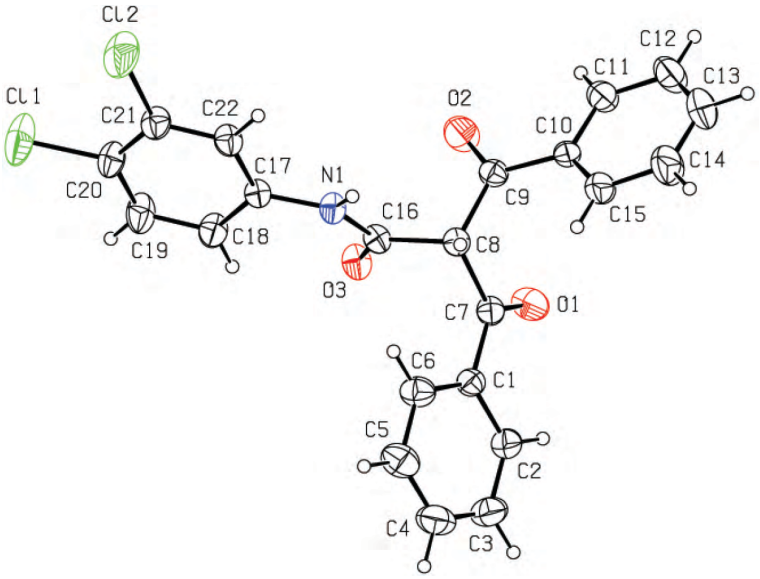

Figure 2. View of the molecular structure of compound **3** with the atom numbering scheme. Displacement ellipsoids for non-H atoms are drawn at the 30% probability level.

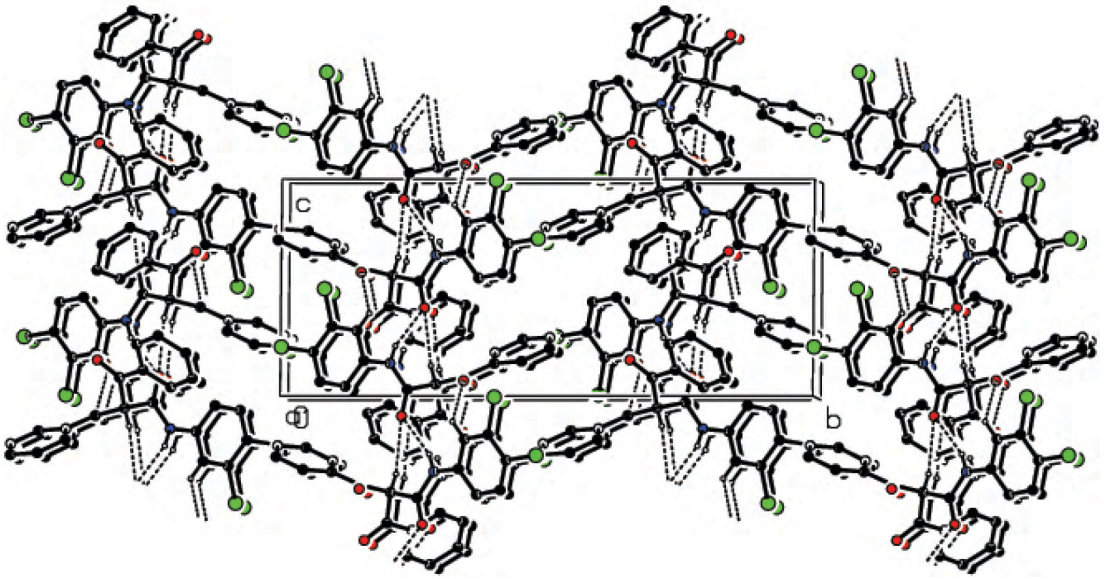

Figure 3. The packing and hydrogen bonding of compound **3**, viewed along the axis. H atoms not involved in hydrogen bonding are omitted.

Table 1. Hydrogen-bond parameters (Å, °).

	D–H	H...A	D...A	D–H...A
N1–H1...O3^{i}	0.86	2.12	2.947 (3)	160
C8–H8...O3^{i}	0.98	2.52	3.213 (3)	127
C18–H18...O3	0.93	2.33	2.870 (4)	117
C22–H22...O2^{i}	0.93	2.51	3.194 (4)	131
C13–H13...Cg3^{ii}	0.93	2.83	3.629 (5)	145

Symmetry codes: (i) x, 1/2 – y, 1/2 + z; (ii) 2 – x, –1/2 + y, 3/2 – z. Cg3 is a centroid of the C17–C22 benzene ring.

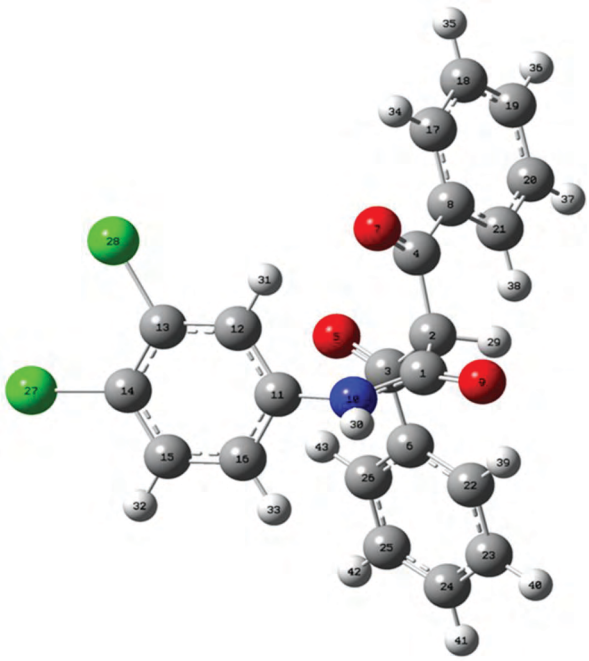

Figure 4. The geometry optimized compound **3** at DFT/B3LYP/SDD basis set in Gaussian09.

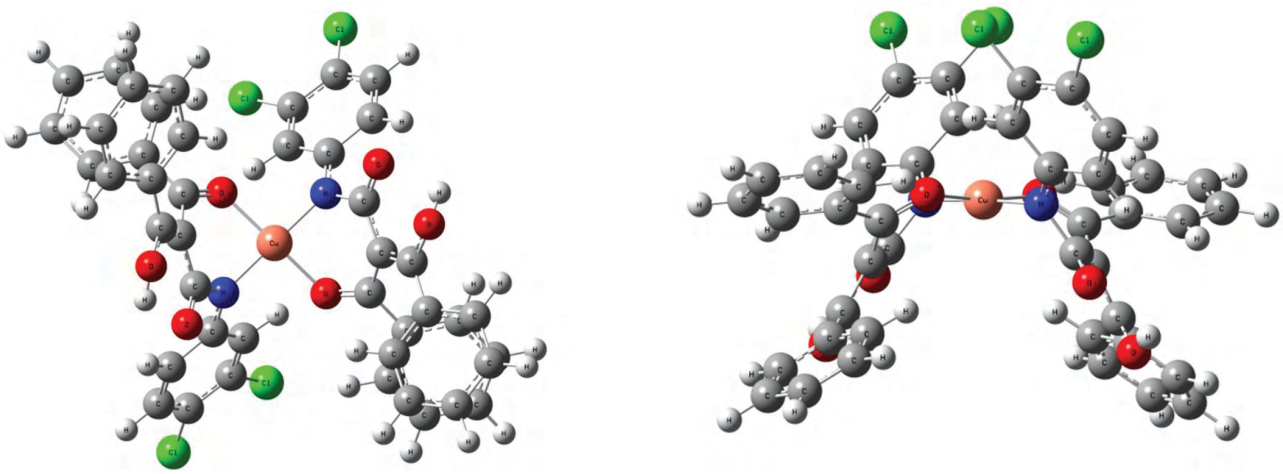

Figure 5. PM6 optimized top and side views of the Cu(II) complex compound **4**, respectively.

2.4. Antimicrobial and antifungal activity results

The bioassay analysis of *N*-(3,4-dichlorophenyl)-3-oxo-3-phenyl-2-(phenyl carbonyl) propanamide (**3**) against the selected bacterial and fungal cultures did not exhibit any significant activities as given in Table S11.

In quantum mechanical calculations, the calculation of atomic charges in any molecule plays an important role in molecular systems. In particular, the charge distributions calculated by the natural bond orbital (NBO) and Mulliken[15] charges for compound **3** are given in Table S12 at the DFT/B3LYP/SDD basis set in this study. This distribution also has an important influence on the vibrational spectra. In the compound *N*-(3,4-dichlorophenyl)-3-oxo-3-phenyl-2-(phenylcarbonyl) propanamide (**3**), the Mulliken atomic charge of the carbon atoms in the neighborhood of C6, C8, and C11 became more positive. This condition of compound **3** demonstrated the direction of delocalization. The natural atomic charges showed more precision with the changes in the molecular structure than Mulliken's net charges. The negative charges mainly located on atoms O9, N10, and C26 will interact with the positive part of any macromolecule-like receptor. These obtained results are presented in Figure 6. In order to evaluate the sensitivity of the calculated charges of compound **3** to changes in the choice of the basis set and the quantum mechanical method, we compared Mulliken charges obtained by different basis sets and this is tabulated in Table S13. In addition, Figure 7 shows the results better in graphical form. We observed that SDD basis set was the most accurate and logical method.

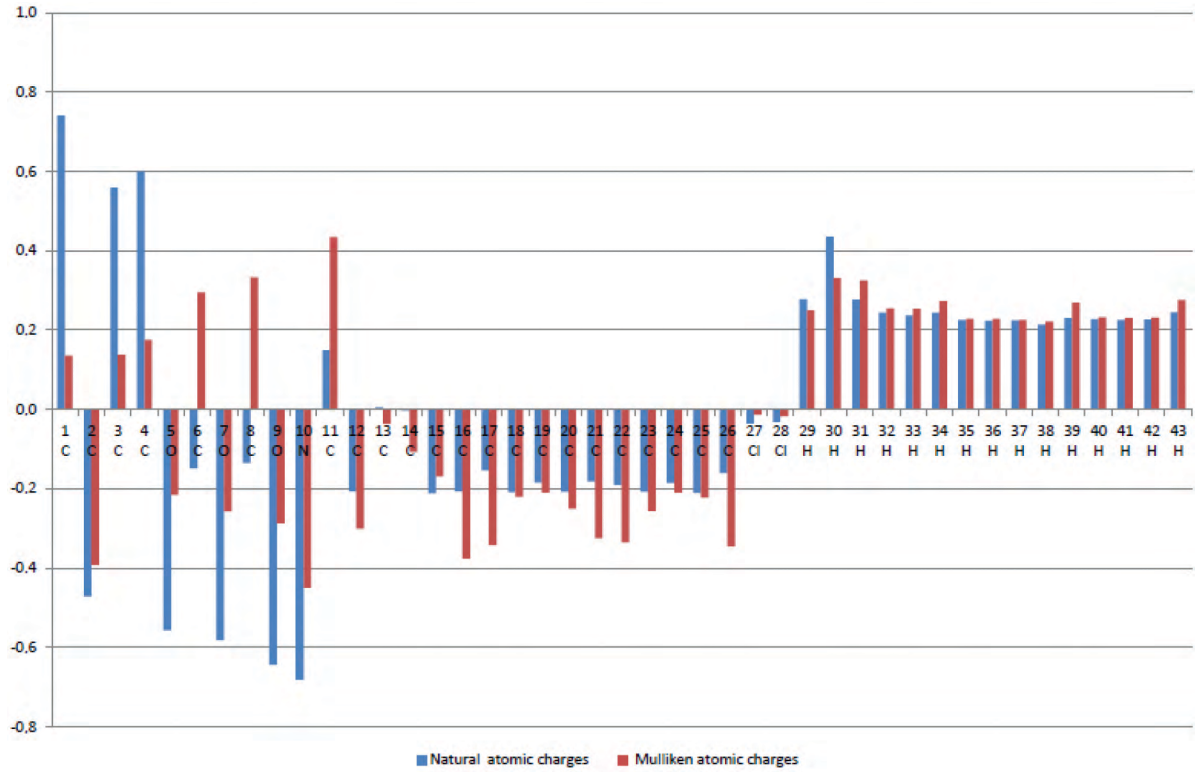

Figure 6. Mulliken's and natural bond orbital's charges plot of compound **3**.

As mentioned, the vibrational analysis for compound **3** was performed with the same basis set by using the G09 program to observe and evaluate the effects of the charge distribution results of compound **3**. The optimized compound **3** belonged to the C1 point group. The vibrational assignments were done on the basis of relative intensities, line shape and the animation option of Gaussview 5.0. When the wavenumber values

were computed at the Hartree–Fock and DFT levels, the obtained results displayed an overestimate of the fundamental modes against the experimental vibrational modes. Scaling factor values of 0.8929 and 0.9613 have been used for HF/6-31G* and DFT[16] hybrid B3LYP functional[17,18] and SDD basis sets to obtain a logical better agreement with experimental data,[19] respectively. The scaled wavenumbers and experimental infrared spectra are displayed in Figure 8.

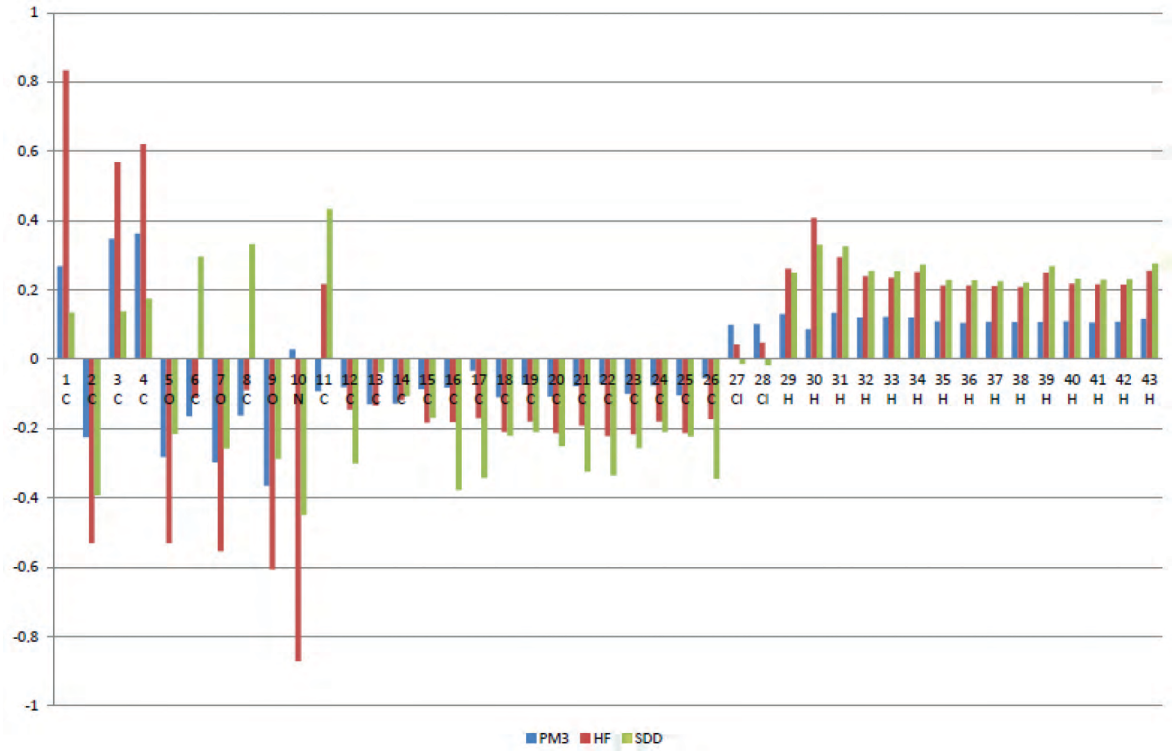

Figure 7. Comparison of different methods for obtained atomic charges of compound **3**.

Amide group vibrations

The most characteristic bands in the spectra of the amide compound are due to the C=O stretching and N–H stretching vibrations. In the amide compound the C=O stretching vibration and N–H stretching vibration are located at 1687, 1672, 1537 cm^{-1} (strong), and 3254 cm^{-1}, respectively. For this study, B3LYP/SDD calculation results indicated that the N–H stretching vibration was at 3254 cm^{-1} for compound **3**. The C=O stretching vibration of amide and ketone groups and the C–H fingerprint region overlapped each other and were located at about 1686, 1682, and 1547 cm^{-1} in the theoretical IR spectrum.

Phenyl ring vibrations

There are three benzene rings, R_1, R_2, and R_3, where R_1 is a part of the amide group and R_2 and R_3 are attached to the carbonyl group of the ketone groups in compound **3**. The calculated wavenumbers for the C–H stretching modes were at 3065 cm^{-1} and have been matched with the experimental IR spectrum (3062 cm^{-1}). Vibrations involving C–H in-plane bending were found throughout the region 1600–997 cm^{-1}. The computed bands at 1595 and 989 cm^{-1} were due to semicircle stretching, and were well matched with experimentally observed bands at 1593 cm^{-1} and 987 cm^{-1} in the IR spectrum. The dominant H–C=C in-plane bending of the R_1, R_2, and R_3 rings was calculated to be at 1612 and 1402 cm^{-1} and corresponded to

the peaks at 1609 and 1392 cm^{-1} in the IR spectrum. The C–H wagging mode started appearing from 680 cm^{-1}, had contributions up to 677 cm^{-1}, and was well assigned in both of the spectra. For ortho substituted benzenes, the C–Cl bending vibrations were also assigned 815 cm^{-1} in the theoretical IR spectrum and 816 cm^{-1} in the experimental IR spectrum.

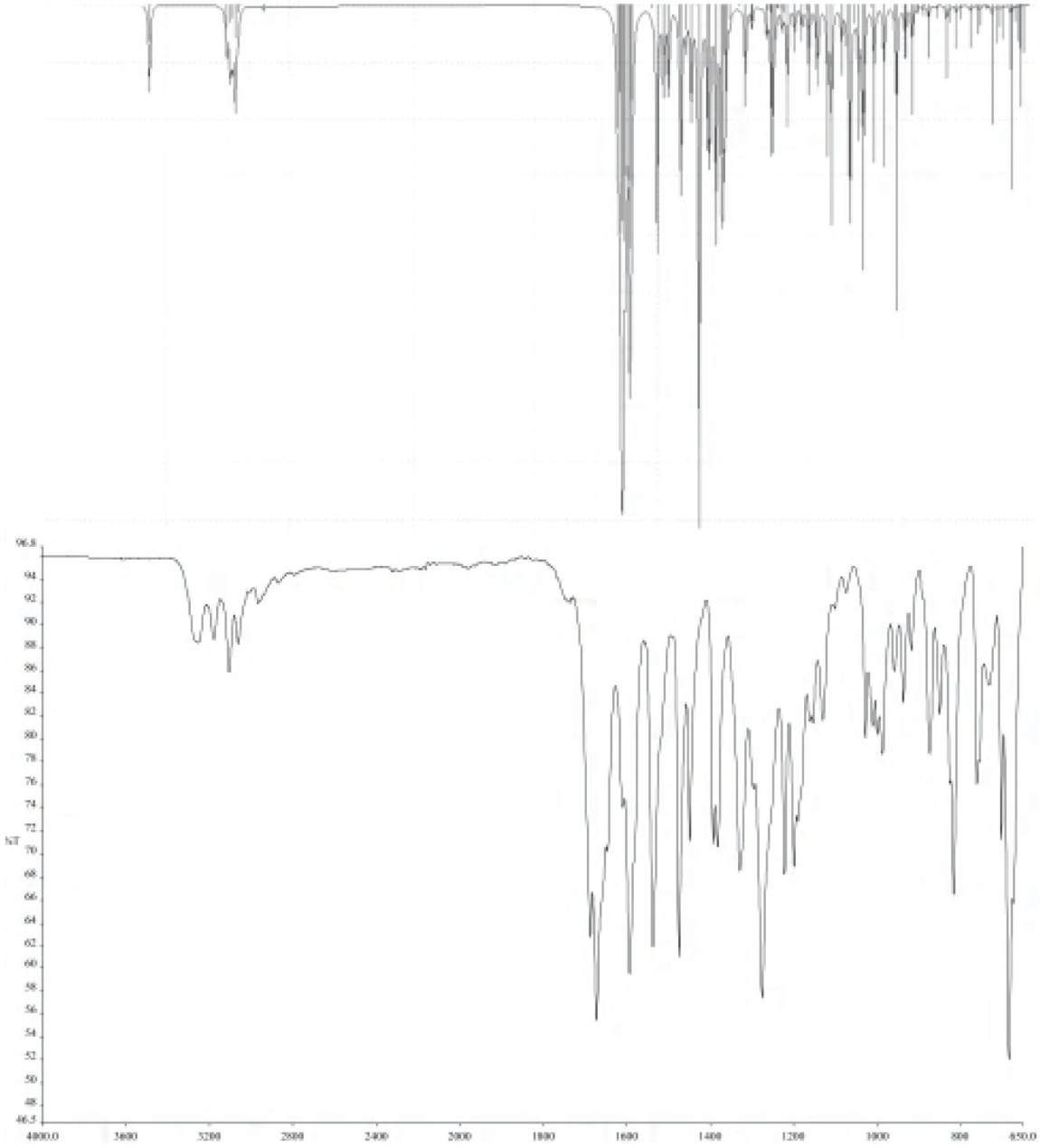

Figure 8. The scaled wavenumbers and experimental infrared spectra of compound **3**.

C=O group vibrations

The appearance of strong bands in the IR spectrum at around 1650–1800 cm^{-1} in aromatic compounds refers to the presence of the carbonyl group and is due to the C=O stretching motion. The wavenumber of the

stretch due to the carbonyl group mainly depends on the bond strength, which in turn depends upon inductive, conjugative, field, and steric effects. The C=O stretching vibrations appeared as strong bands at 1686, 1682, and 1547 cm^{-1} in the theoretical study. The bands in the experimental IR spectrum were located at 1687, 1672, and 1537 cm^{-1}, respectively.

Furthermore, molecular electrostatic potential surface (MEPS) and HOMO–LUMO gap were computed to probe the electron density of compound **3**, prior to formation of the complex compound **4** in the study. MEPS provides a visual method to investigate the correlation between molecular structure and the physiochemical property relationship of molecules such as biomolecules and drugs,[20−26] and to understand sites for electrophilic and nucleophilic reactions like hydrogen bonding interactions.[27,28]

In the present study, the MEPS at the DFT/B3LYP/DD optimized geometry was calculated to predict reactive sites of electrophilic and nucleophilic attacks for compound **3**. The MESP map in the case of compound **3** suggested the potential distribution between carbonyl oxygen atoms (dark red) and nitrogen atoms of amide (dark blue). In the other words, the negative regions (red and yellow) of the MEPS show electrophilic reactivity and the positive (blue) regions nucleophilic reactivity (Figure 9). From the MEPS, it was evident that the negative charge covered the carbonyl oxygen and chloro groups and the positive region was over the nitrogen atom of the amide group. The more electronegativity in the carbonyl oxygen of amide group made it the most reactive part in compound **3**.

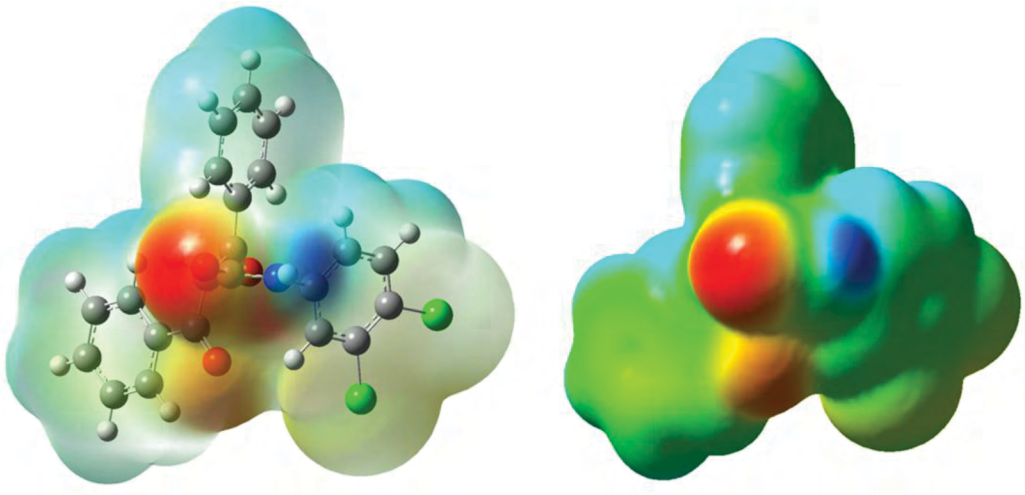

Figure 9. Molecular electrostatic potential map calculated at B3LYP/SDD level for compound **3**.

Additionally, the HOMO–LUMO gap helped us to determine the chemical reactivity and kinetic stability of compound **3**. A high chemical reactivity of a molecule is generally mentioned with a small HOMO–LUMO gap, which is more polarizable and has low kinetic stability. Molecules having these properties are also known as soft molecules.[29]

As stated above, accurate and reliable results can be obtained computationally using several wave function methods such as the second Møller–Plesset perturbation theory (MP2) to examine the band gap and other properties of compound **3**. The HOMO–LUMO gap was used to characterize the conjugated molecule such as the compound *N*-(3,4-dichlorophenyl)-3-oxo-3-phenyl-2- (phenylcarbonyl) propanamide (**3**) at DFT/B3LYP/DD and MP2/6-31G* level in G09. The 3D plots of HOMO and LUMO figures for compound **3** are shown in Figure 10. The HOMO–LUMO gap energy for each method was 4.476 and 10.671 eV, respectively. These

numerical values were also responsible for the bioactive property of compound **3**. These values also validated the antimicrobial and antifungal activity results of this study.

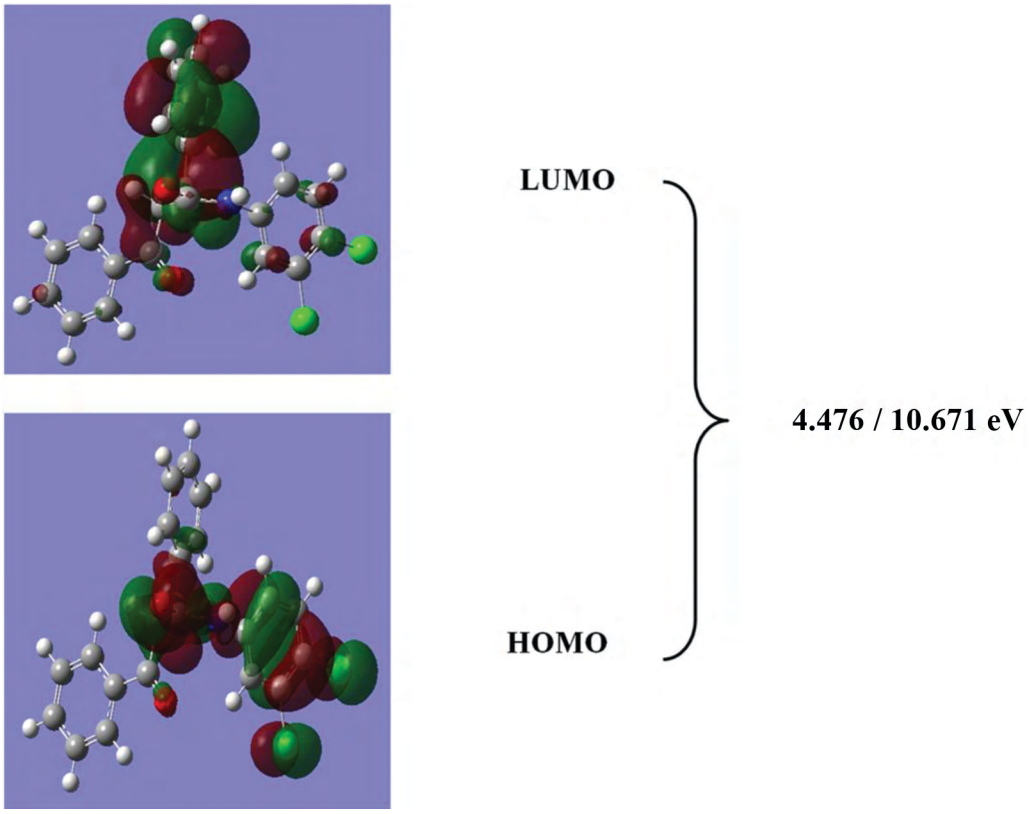

Figure 10. LUMO and HOMO plots of compound **3** at DFT/B3LYP/SDD and MP2/6-31G* level.

After compound **3** was examined, we focused on the complex compound **4** in this part of the study. The complex compound **4** was computed to be square planar at the carboxamide moiety. However, the dichloro phenyl and phenoxy substituents were oriented perpendicular to the main plane and had almost parallel positioning to one another to minimize the steric effects. The phenyl substituents were oriented almost vertical to the main plane. The most stable ground state structure was obtained (Figure 5).

The geometry optimized structures and the Mulliken charge distributions, which are important parameters for compound **4**, are shown in Figures 5 and 11, respectively. Figure 11 indicates a representative charge distribution in the complex compound **4**. The net charge on Cu is 1.256, being lower than the formal charge +2 in Figure 11. This state shows that compound **3** (ligand) transferred its negative charges to Cu(II) ions during formation of the complex compound **4**. All donor atoms of compound **3** also possessed negative charge development. Therefore, the results of geometry optimization and atomic charge showed that there was good agreement between the theoretical and experimental data of the complex compound **4**. The Supplementary Material part also includes detailed information about it in Table S14.

In this part of the study, we explain the biochemical differences among copper, nickel, and zinc complexes. For this purpose, we tried to reveal the biochemical activities of Cu(II), Zn(II), and Ni(II) complex compounds. Firstly, geometrically optimized structures of complex compounds **4**–**6** were obtained at PM6 level of semiempirical basis set in G09 (Figure 12). Additionally, quantum chemical descriptors,[30–33] molecular dipole moment

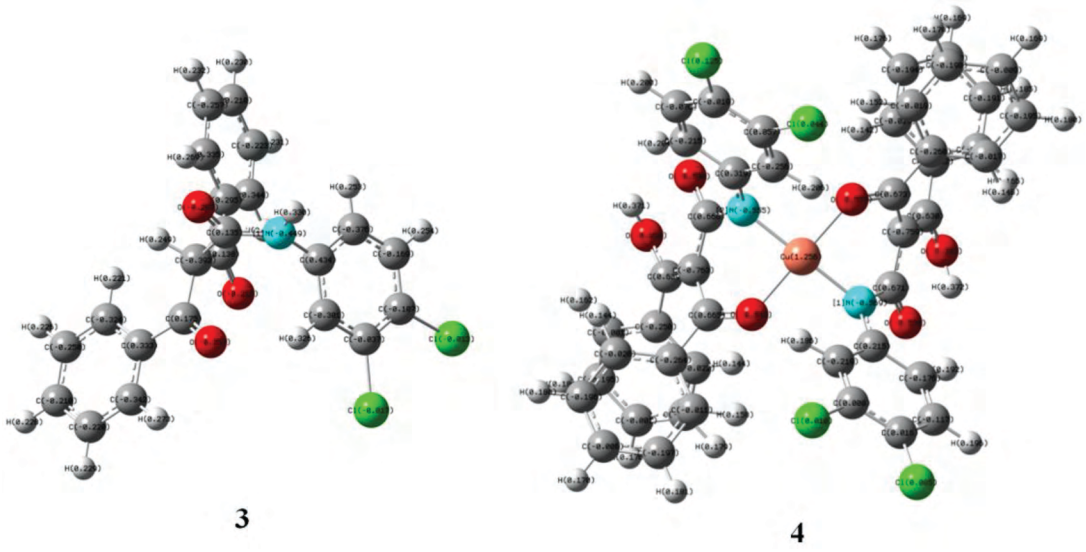

Figure 11. Mulliken charge distributions for compounds **3** and **4**.

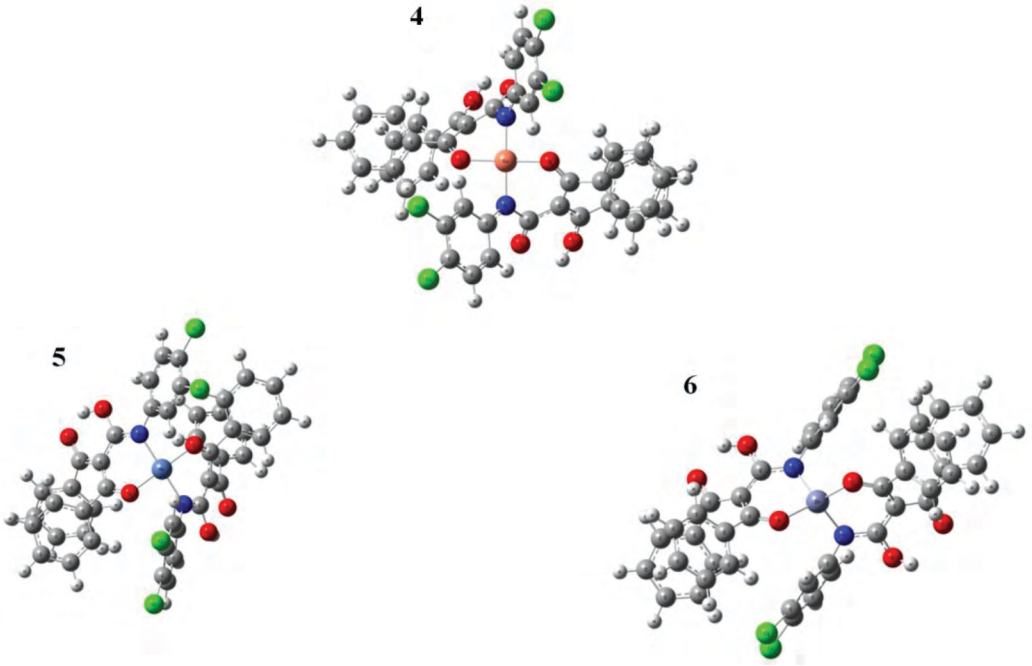

Figure 12. Molecular structures of Cu(II), Ni(II), and Zn(II) coordination complex compounds **4**–**6**.

(μ), energies of the HOMO and LUMO (E_{HOMO}, E_{LUMO}), ionization potential (IP), electron affinity (EA), chemical hardness (μ), softness (S), chemical potential (μ), electronegativity (χ), and electrophilicity index (ω) were used to elucidate some unexplained questions in the experimental part of this study. The obtained structural and electronic information from theoretical calculations at the level of PM6 are shown in Table 2. Furthermore, previous studies[33–35] confirmed electrophilicity index as a possible descriptor of biological activity for different chemical structures. In this study, we focused on the quantum chemical descriptors of the investigated complex compounds (**4**–**6**), because these descriptors helped us to achieve a deeper understanding of the structure activity relationship of the complex compounds **4**–**6**, without the absence of their activity val-

ues. The obtained results indicated that the Cu(II) complex compound has the highest electrophilicity value in all different metal complex compounds, and the mentioned compound (**4**) has higher reactivity and biological activity than the others.

Table 2. Semiempirical theory based descriptors of the metal complex compounds **4**–**6** in G09.

No.	Comp.	(D)	HOMO (eV)	LUMO (eV)	(IP)	(EA)	(η)	(S)	(χ)	(μ)	(ω)
1	**4**	33.054	–0.27732	–0.06864	0.27732	0.06864	0.10434	9.58405	–0.17298	0.17298	0.14339*
2	**5**	3.870	–0.32315	–0.03879	0.32315	0.03879	0.14218	7.03334	–0.18097	0.18097	0.11517
3	**6**	4.147	–0.34883	–0.03527	0.34883	0.03527	0.15678	6.37836	–0.19205	0.19205	0.11763

*Symbol shows the higher biological activities among all compounds. Comp.: compound; D: Molecular dipole moment; I: Ionization potential; EA: Electron affinity; η: Chemical hardness; S: Softness; χ: Electronegativity; μ: Chemical potential; ω: Electrophilicity index; Std: Standard.

Consequently, the new *N*-carboxamide compound **3** and the complex compound **4** were probed by using three stages. In the first stage, they were synthesized and characterized with several techniques. The second stage was used to examine the crystal of the proposed structure **3** not the complex compound **4**, which was in powder state. In the last stage, computational calculations at semiempirical/PM3, HF/6-31G*, and DFT/B3LYP/SDD levels were applied to obtain the optimized three-dimensional geometry of compound **3**. These calculations showed that the DFT/B3LYP/SDD basis set was the most significant and compatible with experimental and X-ray data. It was also observed as the most reactive part in compound **3** with the help of MEPS and HOMO–LUMO energy gap results. At the same time, the complex compound **4** was optimized at semiempirical/PM6 level. The structure and shape of the copper complex compound **4** were confirmed with the help of the results of the Mulliken charge distribution, IR spectra, and magnetic moment value of the complex compound **4**. Moreover, these results will be helpful for the design and synthesis of new carboxamide derivatives and complexes.

3. Experimental

3.1. Chemicals and instrumentation

All chemicals and solvents were purchased from commercial suppliers. The electronic spectrum was recorded on a UV-PG Instruments T80+ UV/Vis spectrometer. The UV pattern was recorded from a 1×10^{-3} molar solution of compounds **3** and **4** dissolved in DMF. The IRνATR spectrum was obtained by PerkinElmer FT-IR/FIR spectrometer between 4000 and 100 cm^{-1} (Gaziantep GU, Chemistry Laboratory, Turkey). APT and ^{1}H NMR spectra for the new *N*-carboxamide compound **3** were obtained with a 400 NMR-PerkinElmer spectrometer using DMSO-d_6 (Gaziosmanpaşa GOU, Chemistry Laboratory, Turkey). All chemical shift values were recorded as δ (ppm). Melting point was measured on an electrothermal apparatus. Elemental analysis results were found to be in good agreement with the calculated data of the mentioned compounds.

3.2. Reactions

3.2.1. Synthesis of compound 3

For the synthesis of *N*-(3,4-dichlorophenyl)-3-oxo-3-phenyl-2-(phenylcarbonyl) propanamide (**3**) (Scheme), a mixture of (1 mmol) dibenzoylaceticacid-*N*-carboxyethylamide (**1**) and (1 mmol) 3,4-dichloroaniline (**2**) was stirred at 150 °C for 3 h in 20 mL of toluene. The solvent was evaporated to dryness and (50 mL) diethyl ether was added to the residue. The solid was filtered, and washed with cold ethanol and diethyl ether. The

pure compound was obtained by recrystallization from n-butanol. White solid, yield: 79%; mp: 193–196 °C. UV-Vis (DMF) λ_{max} nm (log ε): 315.00 (1.737), 270.00 (2.100). IR ν ATR (cm^{-1}): 3254 (m, N–H); 3062 (m, C–H arm); 1687, 1672, 1537 (str, C=O), 1593–1448 (m, C=C), 816 (s, Ph–Cl). ^{1}H NMR (400 MHz, DMSO): δ = 3.40 (1H, C–H), 6.74–8.20 (ArH, m, 13H), 10.73 (1H, s, N–H). APT NMR (100 MHz, DMSO): δ = 64.88, 119.67, 120.78, 125.74, 127.90, 128.86, 129.34, 129.56, 131.37, 131.64, 134.49, 136.00, 139.10, 164.73, 192.75. Chemical formula: $C_{22}H_{15}Cl_2NO_3$; Molecular weight: 411.04; LC-MS/MS (m/z): 413.3 $[M + 2H]^+$; Anal. Calc. for $C_{22}H_{15}Cl_2NO_3$ (%): C, 64.09; H, 3.67; N, 3.40. Found (%): C, 64.32; H, 3.69; N, 3.49.

3.2.2. Synthesis of the complex compounds 4–6

The complexes **4**–**6** were prepared from 206 mg (0.5 mmol) of protonated ligand (**3**) ($C_{22}H_{15}Cl_2NO_3$) dissolved in $CHCl_3/CH_3OH$ (20/10 mL) and 50, 55, and 62 mg (0.25 mmol) of three metal salts [$Cu(CH_3COO)_2.H_2O$, $Zn(CH_3COO)_2.2H_2O$, and $Ni(CH_3COO)_2.4H_2O$] dissolved in a chloroform and methanol mixture, respectively. Cu(II) complex **4** was only carried out in this condition. This case was explained by means of computational techniques. The complex compound **4** was filtered off, washed with methanol and diethylether, and dried in vacuo. Green color powder, yield (81%), mp: 233 °C (decomposition began at value greater than 233 °C. UV-Vis (DMF) λ_{max} nm (log ε): 315 (1.227), 270 (0.932). IR ν ATR (cm^{-1}): 3028 (br, C–H arm); 1617 (str, C=O); 1593–1448 (m, C=C), 1513 (str, C=N); 811 (s, Ph–Cl); μ_{eff}: 1.82 B.M. Chemical formula: $C_{44}H_{28}Cl_4CuN_2O_6$; Molecular weight: 886.06; Anal. Calcd. For $C_{44}H_{28}Cl_4CuN_2O_6$ (%): C, 59.64; H, 3.19; N, 3.16. Found (%): C, 59.2; H, 3.14; N, 3.22.

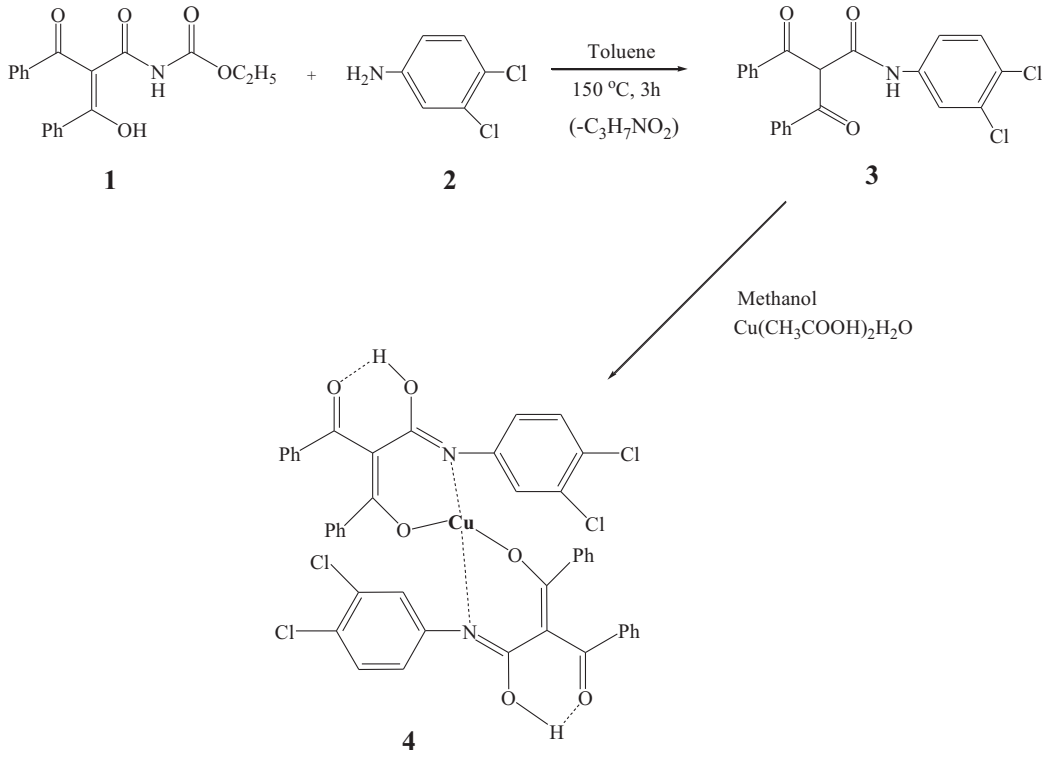

Scheme. The route for the synthesis of compounds **3** and **4**.

3.3. X-ray crystallography

X-ray diffraction data were obtained at 296 K on a Bruker Kappa APEXII CCD diffractometer equipped with graphite monochromated Mo-Kα radiation (λ= 0.71073 Å). The structure was solved by direct methods using SHELXS-97[36] and refined by full matrix least-square on F^2 (SHELXL-97[36]) using anisotropic displacement parameters for all nonhydrogen atoms. All H atoms were positioned geometrically and refined by using a riding model, with N–H = 0.86 Å, C–H = 0.93 and 0.98 Å, and U_{iso}(H) = 1.2U_{eq} (C, N). Figures were drawn using

Table 3. Crystal data and structure refinement for compound **3**.

Chemical formula	$C_{22}H_{15}Cl_2NO_3$
M_r	412.25
Crystal system, space group	Monoclinic, $P2_1/c$
Temperature (K)	296
a, b, c (Å)	9.7704 (13), 22.185 (3), 9.4324 (11)
μ (°)	105.685 (5)
V (Å^3)	1968.4 (4)
Z	4
$F(000)$	848
D_x (Mg m^{-3})	1.391
Radiation type	Mo $K\alpha$
No. of reflections for cell measurement	266
θ range (°) for cell measurement	3.3–21.6
μ (mm^{-1})	0.35
Crystal shape	Prism
Color	Blue
Crystal size (mm)	0.35 × 0.25 × 0.22
Diffractometer	Bruker Kappa APEXII CCD diffractometer
Radiation source	Fine-focus sealed tube
Monochromator	Graphite
Scan method	ω scans
Absorption correction	Multiscan (*SADABS*; Bruker, 2005)
$T_{\min}$, $T_{\max}$	0.900, 0.925
No. of measured, independent and observed [$I > 2\sigma$ (I)] reflections	15,278, 3845, 2215
R_{int}	0.047
θ values (°)	$\theta_{\max}$ = 26.0, $\theta_{\min}$ = 1.8
(sin $\theta/\lambda)_{\max}$ (Å^{-1})	0.617
Range of h, k, l	h = –8→12, k = –27→27, l = –11→10
Refinement on	F^2
$R[F^2 > 2\sigma(F^2)]$, wR (F^2), S	0.054, 0.136, 1.02
No. of reflections	3845
No. of parameters	253
No. of restraints	0
H-atom treatment	H-atom parameters constrained
Weighting scheme	$w = 1/[\sigma^2(F_o^2) + (0.0426P)^2 + 1.0932P]$ where $P = (F_o^2 + 2F_c^2)/3$
$(\Delta/\sigma_{\max}$	< 0.001
$\Delta\rangle_{\max}$, $\Delta\rangle_{\min}$ (e Å^{-3})	0.54, –0.59

the programs PLATON[37] and ORTEP-3.[38] Details of the data collection and the refinement process are given in Table 3.

3.4. Antimicrobial and antifungal activities

Bacillus cereus ATCC 7064, *Staphylococcus aureus* ATCC 6538, *Staphylococcus aureus* ATCC 25923, *Escherichia coli* ATCC 4230, and *Micrococcus luteus* ATCC 9345 were used as the test microorganisms. In addition, *Candida albicans* ATCC 14053, *Candida parapsilosis* ATCC 22019, and *Candida krusei* ATCC 6258 were used to test compound **3** against fungal strains. Compound **3** was examined against gram-negative and gram-positive bacterial and fungal strains as compared to reference compounds, ampicillin and fluconazole, respectively.

3.5. Computational details

All calculations were performed with the Gaussian09 program[39] using the semiempirical/PM3, HF/6-31G*, and DFT/B3LYP/SDD basis sets to optimize the structure of the new *N*-carboxamide compound (**3**). In addition, frequency calculations were applied to confirm the structure as minimum points in energy. In order to do fast and accurate calculations in DFT level, the Stuttgart/Dresden effective core potential basis set (SDD)[40] was also chosen.[41] Moreover, the geometry optimized structure of the obtained complex compound **4** was calculated at the PM6 basis set of the G09 program. The most accurate results were obtained from high-level ab initio calculations with extended basis sets. These types of calculations need the highest computational efforts and are extremely expensive for large molecules containing transition metal elements. On the other hand, semiempirical calculations are fast but have limited reliability. Actual applications have to balance the required accuracy against the available computational resources. The semiempirical method PM6[42] has been considered a practical and effective computational tool, especially for organometallic compounds. The molecular structures were fully optimized in the gas phase, without symmetry. The harmonic frequencies were also calculated to ensure that the optimized structures were in a stable ground state.

Furthermore, there are some unexplained questions in the experimental part; for example, what are the biochemical differences among these complex compounds and so on? Hence molecular modeling of these mentioned structures was performed at PM6 basis set of semiempirical in G09. All calculations were performed with the help of a computer equipped with Intel Core 2 Duo E7600 (3.06 GHz) processors and 4 GB of operating memory.

Acknowledgments

This work was supported by Grant FEF 10.08 financed by Gaziantep Scientific Research Projects. The authors acknowledged the provision of funds for the purchase of a diffractometer and encouragement by Dr Muhammad Akram Chaudhary, Vice Chancellor, University of Sargodha, Pakistan.

Supplementary material

CCDC-997477 contains the supplementary crystallographic data for this paper. These data can be obtained free of charge via http://www.ccdc.cam.ac.uk/conts/retrieving.html, or from the Cambridge Crystallographic Data Centre, 12 Union Road, Cambridge CB2 1EZ, UK; fax: (+44) 1223 - 336 - 033; or e-mail: deposit@ccdc.cam.ac.uk.

References

1. Hranjec, M.; Sovic, I.; Ratkaj, I.; Pavlovic, G.; Ilic, N.; Valjalo, L.; Pavelic, K.; Pavelic, S. K.; Zamola, G. K. *Eur. J. Med. Chem.* **2013**, *59*, 111-119.
2. Strupi, M.; Roatafi, G.; Stables, J. P.; Pruszewski, R. *Acta Pol. Pharm.* **2009**, *66*, 155-159.
3. Sönmez, M. *Turk. J. Chem.* **2001**, *25*, 181-185.
4. Panda, C.; Ghosh, M.; Panda, T.; Banerjee, R.; Gupta, S .S. *Chem. Commun.* **2011**, *47*, 8016-8018.
5. Singh, A. K.; Balamurugan, V.; Mukherjee, R. *Inorg. Chem.* **2003**, *42*, 6497-6502.
6. Noveron,J. C.; Olmstead, M. M.; Mascharak, P. K. *Inorg. Chem.* **1998**, *37*, 1138-1139.
7. Raymond, K. N.; Carrano, C. J. *Acc. Chem. Res.* **1979**, *12*, 183-190.
8. Bhowan, M. G.; Lanlloo, S. J.; Ramnial, T. *Trans. Met. Chem.* **2001,** *26*, 329-332.
9. Millhauser, G. L. *Acc. Chem. Res.* **2004**, *37*, 79-85.
10. Fabian, W. F.; Kollenz, G.; Akcamur, Y.; Kök, T. R.; Tezcan, M.; Akkurt, M.; Hiller, W. *Monath. Chem.* **1992**, *123*, 265-275.
11. Bhaskare, C.; Hankare, P. P.; *J. Indian Chem. Soc.* **1995**, *72*, 585-587.
12. Nishat, N.; Rahis ud-din, Haq, M. M.; *Pol. J. Chem.* **2003**, *77*, 1731– 1740.
13. Allen, F. H.; Kennard, O.; Watson, D. G.; Brammer, L.; Orpen, A. G.; Taylor, R. *J. Chem Soc. Perkin Trans II:* **1987,** S1-19.
14. Bernstein, J.; Davis, R. E.; Shimoni, L.; Chang N. L. *Angew Chem Int Ed Engl* **1995**, *34*, 1555–1573.
15. Mulliken, R. S. *J. Chem. Phys.* **1955**, *23*, 1833–1840.
16. Becke, A. D. *J.Chem. Phys.* **1993**, *98*, 5648-5652.
17. Lee, C.; Yang, W.; Parr, R. G. *Phys. Rev. B.* **1988**, *37*, 785-789.
18. Hohenberg, P.; Kohn, W. *Phys. Rev. B.* **1964**, *136*, 864-871.
19. Foresman, J. B. in: E. Frisch (Ed.), Exploring *Chemistry with Electronic Structure Methods:* A Guide to Using Gaussian, Gaussian, Inc., Pittsburg, PA, **1996**.
20. Murray, J. S.; Sen, K. *Molecular Electrostatic Potentials, Concepts and Applications,* Elsevier, Amsterdam, **1996**.
21. Alcorta, I.; Perez, J. J. *Int. J. Quant. Chem.* **1996**, *57*, 123-135.
22. Scrocco, E.; Tomasi, J. *Advances in Quantum Chemistry*, ed. P. Lowdin, Academic Press, New York, **1978,** 115-143.
23. Luque, F. J.; Orozco, M.; Bhadane, P. K.; Gadre, S. R. *J. Phys. Chem.* **1993**, *97*, 9380-9384.
24. Sponer, J.; Hobza, P. *Int. J. Quant. Chem.* **1996**, *57*, 959-970.
25. Pathak, R. K.; Gadre, S. R. *J. Chem. Phys.* **1990**, *93*, 1770-1773.
26. Gadre, S. R.; Shrivastava, I. H. *J. Chem. Phys.* **1991**, *94*, 4384-4390.
27. Scrocco, E.; Tomasi, J. *Adv. Quantum. Chem.* **1978**, *11*, 115–193.
28. Luque, F. J.; Lopez, J. M.; Orozco, M. *Theor. Chem. Acc.* **2000**, *103*, 343–345.
29. Fleming, I. *Frontier Orbitals and Organic Chemical Reactions,* John Wiley and Sons, New York, **1976**.
30. Parr, R. G.; Szentpaly, L. V.; Liu, S. *J. Am. Chem. Soc.* **1999**, *121*, 1922-1924.
31. Maynard, A. T.; Huang, M.; Rice, W. G.; Covell, D. G. *Proc. Natl. Acad. Sci.* USA, **1998**, *95*, 11578-11583.
32. Chattaraj, P. K.; Giri, S.; Duley, S. *Chem. Rev.* **2011**, *111*, 43-75.
33. Taskin, T.; Sevin, F. *J. of Mol. Struc.: Theochem* **2007**, *803*, 61–66.
34. Parthasarathi, R.; Subramanian, V.; Royb, D. R.; Chattaraj, P. K. *Bioorg. and Med. Chem.* **2004**, *12*, 5533–5543.
35. Taskin, T.; Sevin, F. *Turk. J. Chem.* **2011**, *35*, 481-498.

36. Sheldrick, G. M. *Acta. Cryst.* **2008,** *A64*, 112–122.

37. Farrugia, L. J. *J. Appl .Cryst.* **1997**, *30*, 565-566.

38. Spek, A. L. *Acta Cryst.* **2009,** *D65*, 148–155.

39. Gaussian 09, Revision C.01, Frisch, M. J.; Trucks, G. W.; Schlegel, H. B.; Scuseria, G. E.; Robb, M. A.; Cheeseman, J. R.; Scalmani, G.; Barone, V.; Mennucci, B.; Petersson, G. A.; et. al. Gaussian, Inc., Wallingford CT, **2011**.

40. Hay, P. J.; Wadt, W. R. *J. Chem. Phys.* **1985**, *82*, 270–283.

41. Zhao, J. Y.; Zhang, Y.; Zhu, L. G. *J. Mol. Struct. Theochem.* **2004**, *671*, 179–187.

42. Stewart, J. J. P. *J. Mol. Model.* **2007**, *13*, 1173-213.